IJMSO

International Journal of Mathematical Sciences and Optimization: Theory and Applications
11(4), 2025, Pages 123 - 137
https://doi.org/10.5281/zenodo.19005495

# An Analytical Investigation of MHD Williamson Fluid Flow over an Inclined Stretching Sheet in a Porous Medium with Non-Uniform Internal Heat Generation and Mixed Convection

T. A. Oyeyinka [1], R. A. Oderinu [1], S. Alao [1*], B.A. Sanusi [1], F.J. Ayanbukola [1]

1. Department of Mathematics, Ladoke Akintola University of Technology, P.M.B 4000, Ogbomoso, Nigeria.
* Corresponding author: salao16@lautech.edu.ng

**Article Info**
Received: 25 August 2024 Revised: 16 July 2025
Accepted: 26 September 2025 Available online: 02 March 2026

**Abstract**

The complex interplay between heat transfer, fluid motion, and porous media permeability plays a pivotal role in numerous physical and engineering applications. In particular, the control of heat generation and absorption under mixed convection has garnered considerable attention due to its relevance in thermofluid systems embedded in permeable structures. This research presents a semi-analytical approach for solving the nonlinear Williamson fluid model, accounting for the combined effects of mixed convection, medium permeability, and non-uniform heat generation. Through similarity transformations, the governing partial differential equations are reduced to a system of ordinary differential equations, which are subsequently solved using Legendre polynomials as basis functions and Gauss-Lobatto collocation points. The resulting algebraic system is handled in Mathematica 11.0, with solution accuracy verified by comparison to results from the classical Runge-Kutta shooting technique. Numerical findings reveal that increasing the Grashof number enhances fluid velocity, while higher porosity intensifies thermal fields but suppresses flow due to increased resistance in the porous medium. Moreover, spatially varying heat generation induces steep thermal gradients, potentially leading to localized thermal stresses. The proposed methodology proves effective for analyzing complex nonlinear fluid dynamics, offering robust insights for applications in energy systems, geophysical flows, and thermal engineering.

**Keywords:** Williamson fluid, Mixed convection, Non-uniform internal heat generation, Legendre Collocation.
**MSC2010: 76A05.**

## 1 Introduction

Non-Newtonian fluids exhibit complex flow behaviors distinct from classical Newtonian fluids, where viscosity remains consistent regardless of shear rate. Of the various non-Newtonian fluids, the

IJMSO
International Journal of Mathematical Sciences and Optimization: Theory and Applications
11(4), 2025, Pages 123 - 137
https://doi.org/10.5281/zenodo.19005495

Williamson fluid model is especially relevant, representing pseudoplastic fluids that exhibit shear-thinning behavior. This model, introduced by Williamson in 1929 and explored by researchers such as Mansoor et al. [1], Ali et al. [2], and Alzu'bi et al. [3], describes fluids whose viscosity decreases with increased shear rate. This characteristic is significant for applications involving complex fluid dynamics, from biological systems to industrial processes. Over time, the Williamson model has been further refined by studies like those of Alwawi et al. [4] and Gireesha et al. [5], establishing various mathematical frameworks that capture the nuanced behavior of such fluids under diverse conditions.

In a study by Rosli et al. [6], the flow of blood with ferroparticles over a stretching surface was examined using a hybrid Williamson ferrofluid model. Findings demonstrated that as the Williamson fluid parameter, which gauges the ratio of relaxation to retardation time, increased, velocity decreased and boundary layer thickness expanded. This research underlines the model's biomedical applications, especially in analyzing blood flow dynamics. Further studies on Williamson fluid models have incorporated physical effects to expand its applicability. For instance, Ahmed et al. [7] simplified complex equations using similarity transformations, allowing for semi-analytical solutions. Anagandula and Reddy [8] investigated the role of velocity and thermal slips in the flow of Williamson fluids over a stretching sheet with the effects of an inclined magnetic field and radiation.

Recent research on mixed convection effects in Williamson fluid flows emphasizes the role of factors like thermal radiation, chemical reactions, and viscous dissipation. Collectively, these studies enhance our understanding of the behavior of non-Newtonian fluids in mixed convection contexts, contributing to future research and practical applications in thermal management systems. A recent study by Alizadeh et. al [9] explores, for the first time, the mixed convection behavior of CuO-water nanofluid impinging on a heated cylinder embedded in porous media and subjected to a uniform magnetic field. Also, a computational study by Ibrahim and Gamachu [10] investigates the mixed convection flow of Williamson nanofluid past a radially stretching surface, incorporating the effects of first-order velocity slip and convective boundary conditions. Maleque [11], examined the similarity requirements for three-dimensional combined forced and free convective laminar boundary layer flows over porous, inclined vertical curvilinear surfaces. The study incorporates buoyancy and heat absorption/generation effects, focusing on incompressible fluid flow. Oderinu et. al [12] explored the effects of internal heat generation/absorption and unsteady mixed convection flow of a micropolar fluid through a permeable channel, an area of critical interest for thermal management in industries such as chemical processing, mechanical systems, oil exploration, and aeronautical engineering. Also, a recent study by Panezai et al. [13] investigates the impact of thermal radiation on the two-dimensional incompressible magnetohydrodynamic (MHD) mixed convection flow of Williamson fluid over a porous wedge. The research employs similarity transformations to simplify the boundary layer partial differential equations into a system of nonlinear ordinary differential equations. Raji et al. [14] explored an analytical and numerical study on the influence of carbon nanotubes in magnetohydrodynamic (MHD) mixed convection nanofluid flow over an inclined plate with a constant wall temperature. The study focuses on two types of nanofluids: SWCNT/kerosene and MWCNT/kerosene.

Studies on non-uniform heat generation in MHD fluid flow have revealed the interdependent dynamics of non-Newtonian fluids subjected to magnetic fields and varying thermal conditions. Williamson fluids as a case study respond significantly to thermal gradients and external forces, making them a focal point in fluid dynamics research. Akter [15] explored the unsteady flow of Williamson fluids over an exponentially stretching sheet, accounting for non-uniform heat generation and an inclined magnetic field; The results indicated that non-uniform heat generation impacts the thermal boundary layer, affecting temperature distribution and flow behavior. This aligns with findings from Jyotshna and Dhanalaxmi [16], who observed that a heat source increases the boundary layer thickness and reduces the heat transfer rate from surface to fluid. Furthermore, findings from Alao et al [17] revealed that the presence of a heat source significantly enhances the temperature profile due to intensified viscous heating. Kumar et al. [18] also contributed by examining non-uniform heat sources and Joule heating's impact on MHD micropolar fluids,

IJMSO

International Journal of Mathematical Sciences and Optimization: Theory and Applications
11(4), 2025, Pages 123 - 137
https://doi.org/10.5281/zenodo.19005495

underscoring the significance of both space- and temperature-dependent heat sources in shaping fluid flow and thermal profiles. A study by Raju et al, [19] showed that a space- and temperature-dependent heat source significantly boosts heat transfer in Casson fluid compared to Williamson fluid, highlighting its effectiveness in controlling thermal behavior. A further study by Swain et al, [20] on MHD boundary layer flow of Williamson nanofluid reveals that a non-uniform heat source and higher Eckert number enhance the heat transfer rate, while simultaneously reducing the mass transfer rate, especially in porous media with melting effects. Further studies highlight the substantial impact of non-uniform heat generation on MHD Williamson fluid dynamics, stressing the complex interplay of thermal gradients, magnetic fields, and fluid properties. These insights inform more effective thermal management strategies for engineering applications.

Recent advancements in semi-analytical methods, particularly those employing polynomials and collocation techniques, have advanced numerical solutions for various complex mathematical models in fluid dynamics. The study by Alao et al, [21] employed a collocating weighted residual scheme to simulate the analytical solution of viscous heating and thermal gyration in magneto-micropolar fluid flow with internal non-uniform heat generation/absorption; To validate the accuracy of the results, several control methods were used, including the Runge-Kutta shooting method (order four), Adomian decomposition technique, variational iteration scheme, differential transform method, and quasi-linearization technique. By utilizing orthogonal polynomial properties, the semi-analytical methods provide precise approximations for challenging differential equations. Jebreen [22], applied Müntz–Legendre polynomials to solve fractional gas dynamics equations, showcasing the efficiency of Legendre polynomials in fractional differential equations and underscoring their adaptability for systems governed by fractional dynamics. The study by Sanusi et al [23] numerically investigated MHD micropolar Casson fluid flow over a linearly stretching sheet within a porous medium, focusing on mixed convection and heat sources/sinks; A key aspect of the work is the use of Hermite collocation, where Hermite polynomials serve as basis functions in a collocating weighted residual method, with Gauss-Lobatto nodes employed for spatial discretization.

In another significant study, Yousefi et al. [24] proposed a computational method for solving fractional integral equations using Legendre collocation. This method's convergence was tested on second-order fractional integral equations, demonstrating favorable convergence rates when using Gauss-Legendre-Lobatto points. Similarly, Molla and Saha [25] applied Galerkin and collocation methods to approximate solutions for Fredholm integral equations, achieving strong alignment with exact solutions. Legendre polynomial-based semi-analytical methods have proven effective in a broad range of applications in fluid dynamics and integral equations, delivering efficient and accurate numerical results. Olabode [26] examined numerical block methods that accurately and convergently solve second order singular boundary value problems while bypassing initial point singularities. Binta [27] developed a numerical collocation based scheme for solving systems of linear integro differential equations under mixed conditions, transforming the governing equations into linear algebraic systems solved via MATLAB. A study by Demir et al. [28] applied the Legendre operational matrix method based on collocation points to solve high-order nonlinear ordinary differential equations common in physics and mechanics. The method's effectiveness is demonstrated through test problems and residual error estimates, with numerical results validating its accuracy and applicability.

This study builds on foundational research to explore the effects of mixed convection, non-uniform heat generation on Williamson fluid flow over a stretching sheet, influenced by an inclined magnetic field. Legendre polynomials with Gauss-Lobatto collocation points were chosen to solve the system of equations due to their strong convergence properties and efficiency in solving boundary value problems with high accuracy. Governing partial differential equations (PDEs) are transformed into ordinary differential equations (ODEs) and solved using the shooting method in conjunction with the Runge-Kutta approach for various parameter values to validate the accuracy of the semi-analytical method.

IJMSO
International Journal of Mathematical Sciences and Optimization: Theory and Applications
11(4), 2025, Pages 123 - 137
https://doi.org/10.5281/zenodo.19005495

## 2 Formulations of the Model

This research explores the steady, two-dimensional, laminar flow of a Williamson fluid between two parallel, permeable porous walls with a surface stretching with $U_w(x) = bx$. Figure 1 presents the configuration of magnetohydrodynamic (MHD) inviscid flow, accompanied by thermal and concentration boundary layers. The investigation follows the principles of boundary layer theory, applied to a surface stretching with velocity $U_w(x) = bx$, where $b$ is a constant. The surface maintains a temperature $T_w$, while the fluid temperature at a distance from the surface tends toward $T_\infty$. The flow involves Williamson fluid behavior, and the region of interest lies in the domain $y > 0$. A magnetic field is externally imposed, inclined at an angle $\alpha$ with respect to the x-axis. The effect of the induced magnetic field is considered negligible when compared to the externally applied field. This configuration is intended to capture the key flow, heat, and mass transfer characteristics, as illustrated by Anagandula and Reddy [8] in figure 1:

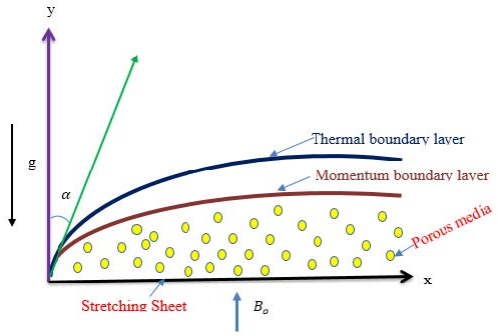


Fig. 1 Flow geometry

The governing equations for fluid dynamics in this study build upon foundational models, notably extending the work of Anagandula and Reddy [8]. In this approach, the momentum equation is refined to account for mixed convection, allowing both temperature and concentration gradients to influence the flow. The energy equation is further adapted to include the effects of permeability within a porous medium, capturing the intricate heat transfer behavior along with non-uniform heat generation effects. These non-uniform heat generation parameters add layers of complexity, introducing localized heating variations that intensify thermal gradients and affect temperature distribution. Additionally, the concentration equation, adapted from Alao et al. [29], encompasses diffusion and reaction dynamics within the flow. The incorporation of concentration effects introduces mass transfer phenomena into the system, where solutal buoyancy can either enhance or oppose convective motion depending on the concentration gradient. This robust model integrates fluid mechanics, heat transfer, and mass diffusion principles, offering a detailed representation of non-Newtonian Williamson fluid flow influenced by various physical forces and parameters.

$$\frac{\partial U}{\partial x} = -\frac{\partial V}{\partial y}, \tag{2.1}$$

$$U\frac{\partial U}{\partial x} + V\frac{\partial U}{\partial y} - \nu\frac{\partial^2 V}{\partial y^2} = \sqrt{2}\nu\Gamma\frac{\partial U}{\partial y}\frac{\partial^2 U}{\partial y^2} - \frac{\sigma B_0^2}{\rho_f}sin^2(\alpha)U - \frac{\nu}{K^*}U + B_t(T - T_\infty)g + B_c(C - C_\infty)g, \tag{2.2}$$

$$U\frac{\partial T}{\partial x} + V\frac{\partial T}{\partial y} = \frac{k}{(\rho C_p)_f}\frac{\partial^2 T}{\partial y^2} + \frac{1}{(\rho C_p)_f}\frac{16\sigma^* T_\infty^3}{3K^*}\frac{\partial^2 T}{\partial y^2} + \frac{\sigma\beta_0^2}{(\rho C_p)_f}U^2 + \frac{\nu}{C_p}\left[\left(\frac{\partial U}{\partial y}\right)^2 + \sqrt{2}\Gamma\left(\frac{\partial U}{\partial y}\right)^3\right] + Q_0(T - T_\infty) + \frac{\nu}{\rho C_p K^*}u^2 + \frac{q'''}{\rho C_p}, \tag{2.3}$$

IJMSO
International Journal of Mathematical Sciences and Optimization: Theory and Applications
11(4), 2025, Pages 123 - 137
https://doi.org/10.5281/zenodo.19005495

$$U\frac{\partial C}{\partial x} = -V\frac{\partial C}{\partial y} + D\frac{\partial^2 C}{\partial^2 y} - K_n(C - C_\infty), \tag{2.4}$$

According to Ayanbukola et al. [30], the non-uniform internal heat generation in 2.3 can be expressed as 2.5:

$$q''' = \frac{k_f u_w}{\nu x}[e_1(T - T_\infty) + e_2(T_w - T_\infty)F'], \tag{2.5}$$

where $e_1$ and $e_2$ are temperature dependent and heat generation space respectively. If $e_1 > 0$, $e_2 > 0$ it is called heat generation but if otherwise it is called heat absorption.

The associated boundary conditions with the governing equations 2.1 to 2.4 given in the work of Anagandula and Reddy [7] as:

$$\left.\begin{aligned} U_w = U = bx + A^*\frac{\partial U}{\partial y}, V = V_w, T = T_f + B^*\frac{\partial T}{\partial y}, C = C_f + X^*\frac{\partial C}{\partial y} \text{as y} \to 0, \\ u = 0, T = T_\infty, C = C_\infty \text{as y} \to \infty \end{aligned}\right\} \tag{2.6}$$

Similarity variables is given as follows:

$$\left.\begin{aligned} \eta = y\left(\frac{b}{\nu}\right)^{1/2}, \quad U = bxF'(\eta), \quad V = -(b\nu)^{1/2}F(\eta), \\ \bar{\theta}(\eta) = \frac{T - T_\infty}{T_w - T_\infty}, \quad \bar{\phi}(\eta) = \frac{C - C_\infty}{C_w - C_\infty}. \end{aligned}\right\} \tag{2.7}$$

By using equation 2.7, the formulated equations 2.2-2.5 are now reduced to dimensionless form:

$$(1 + \lambda\bar{F}'')\bar{F}''' + \bar{F}\bar{F}'' - (\bar{F}')^2 - (Msin^2(\alpha) + K_p)\bar{F}' + Gr\theta + Gm\bar{\phi} = 0 \tag{2.8}$$

$$\bar{\theta}'' + \frac{Pr}{(1+R)}\left[\bar{F}\bar{\theta}' + Ec\left((\bar{F}'')^2 + We(\bar{F}'')^3 + M\bar{F}'^2 + K_p\bar{F}'^2\right) + Q\bar{\theta}\right] + e_1F' + e_2\theta = 0 \tag{2.9}$$

$$\bar{\phi}'' + Sc\big(\bar{F}\bar{\phi}' - Kn\phi\big) = 0 \tag{2.10}$$

The transformed boundary conditions are given as:

$$\left.\begin{aligned} \bar{F}'(\eta) = 1 + A\bar{F}''(0), \bar{F}(\eta) = \bar{F}_w, \bar{\theta}(0) = 1 + \delta\bar{\theta}'(0), \bar{\phi}(0) = 1 + \beta\bar{\phi}'(0) \text{ as } \eta \to 0 \\ \bar{F}'(\eta) \to 0, \bar{\theta}(\eta) \to 0, \bar{\phi}(\eta) \to 0, \text{ as } \eta \to \infty \end{aligned}\right\} \tag{2.11}$$

The parameters used in this study are defined as follows: The magnetic parameter, $M = \frac{\sigma B_0^2}{b\rho_f}$, quantifies the magnetic effects on the flow, while $\lambda = U_w\Gamma(\frac{2b}{\nu})^{1/2}$ represents Williamson parameter. Radiative effects are captured by the term $R = \frac{16\sigma T_\infty^3}{3kk^*}$, and the Weissenberg number is characterized by the term $We = x\Gamma(\frac{2b^3}{\nu})^{1/2}$. The Prandtl number, $Pr = \frac{k}{\rho C p_f}$, relates the fluid's viscosity to its thermal diffusivity, whereas the Eckert number, $Ec = \frac{u_w^2}{C_p(T_f - T_\infty)}$, indicates the ratio of kinetic energy to thermal energy.

The Schmidt number, $Sc = \frac{\nu}{D_b}$, describes the relative rates of momentum and mass diffusion, while the suction/injection constraint is given by $\bar{F}_w = \frac{V_w}{(b\nu)^{1/2}}$. The velocity slip, thermal slip, and mass slip are represented by $A = A^*(\frac{b}{\nu})^{1/2}$, $\delta = B^*(\frac{b}{\nu})^{1/2}$, and $\beta = X^*(\frac{b}{\nu})^{1/2}$, respectively. Buoyancy effects in thermal and concentration contexts are defined by the Grashof number, $Gr = \frac{\beta_t(T_w - T_\infty)bg}{U_w}$, and the modified Grashof number, $Gm = \frac{\beta_c(C_w - C_\infty)bg}{U_w}$. Permeability within the porous medium is characterized by $K_p = \frac{\nu}{bk^*}$, while the heat source parameter is given by $Q = \frac{Q_o}{\rho C_p}$.

The local skin friction coefficient, $C_{fx}$, as derived from equation 2.6, is expressed as:

$$C_{fx} = \frac{\tau_w}{\rho U_w^2} = \left(1 + \frac{\lambda}{2}F''(0)\right)f''(0) \tag{2.12}$$

IJMSO

International Journal of Mathematical Sciences and Optimization: Theory and Applications
11(4), 2025, Pages 123 - 137
https://doi.org/10.5281/zenodo.19005495

where the shear stress at the wall, $\tau_w$, is defined by:

$$\tau_w = \left[\frac{\partial U}{\partial y} + \frac{\Gamma}{\sqrt{2}}\left(\frac{\partial U}{\partial y}\right)^2\right]_{y=0} \tag{2.13}$$

and the thermal flux at the wall is represented as:

$$q_w(x) = -k\left(\frac{\partial T}{\partial y}\right)_{y=0} + (q_r)_{y=0}. \tag{2.14}$$

Additionally, based on the similarity variables in equation 2.6, the Nusselt number $Nu_x$ is given by:

$$Nu_x = \frac{xq_w}{k(T - T_w)} = -(1 + R)\theta'(0) \tag{2.15}$$

# 3 Numerical Approach

The analytical solution for equations 2.8-2.10 leverages the Legendre polynomial method, using shifted Gauss-Lobatto points as collocation nodes. This approach involves interpolating over discrete sub-intervals by selecting a trial function, generally an exponential or polynomial, to approximate the solution of a differential equation over the interval $a_0 \leq x \leq b_0$. According to Akolade et.al [31], the shifted Gauss-Lobatto points is defined as:

$$\eta_k = \frac{\eta_L}{2}\left(1 - Cos\left(\frac{k\pi}{N}\right)\right), \text{for } k = 0, 1, 2, ..., n. \tag{3.1}$$

The trial function, applied at chosen nodes, enables the formulation of a system of equations to determine the coefficients. In this study, the functions $\bar{f}$, $\bar{\theta}$, and $\bar{\phi}$ serve as trial functions in this procedure as outlined below:

$$\bar{F} = LegendreP\sum_{k=0}^{n} a_k\left(\frac{2\eta}{\eta_\infty} - 1\right) \tag{3.2}$$

$$\bar{\theta} = LegendreP\sum_{k=0}^{n} b_k\left(\frac{2\eta}{\eta_\infty} - 1\right) \tag{3.3}$$

$$\bar{\phi} = LegendreP\sum_{k=0}^{n} c_k\left(\frac{2\eta}{\eta_\infty} - 1\right) \tag{3.4}$$

The coefficients $a_k$, $b_k$, and $c_k$, represent the unknowns to be identified, here $k = 0, 1, 2, \ldots, n$, with $n$ representing the convergence point of the solution. Also, the boundary conditions, as transformed in equation (11), are applied to the base functions in equations (8)-(10), forming a system of algebraic equations. Residuals, namely $\bar{F}_{res}$, $\bar{\theta}_{res}$, and $\bar{\phi}_{res}$, are then derived by substituting equations (15)-(17) into equations (8)-(10) and collocating at Gauss-Lobatto points. These coefficients $[a_k, b_k, c_k \mid k = 0, 1, \ldots, n]$ are defined as polynomials aimed at minimizing residual errors. Using Mathematical software , the unknown coefficients are substituted back into the trial functions 3.2-3.4, allowing for the transformation of equations 2.8-2.10 into:

$$\begin{aligned}\bar{F}(\eta) = 0.688454 + 0.134473(-2+\eta) - 0.027513(8-12\eta+3\eta^2) + 0.00465727(-16+48\eta-30\eta^2+5\eta^3) \\ - 0.000134074(128 - 640\eta + 720\eta^2 - 280\eta^3 + 35\eta^4) + \\ 0.0000301773(-256 + 1920\eta - 3360\eta^2 + 2240\eta^3 - 630\eta^4 + 63\eta^5)\end{aligned} \tag{3.5}$$

IJMSO

International Journal of Mathematical Sciences and Optimization: Theory and Applications
11(4), 2025, Pages 123 - 137
https://doi.org/10.5281/zenodo.19005495

$$\bar{\theta}(\eta) = 0.24128 - 0.213693(-2+\eta) + 0.0303866(8 - 12\eta + 3\eta^2) - 0.00291187(-16 + 48\eta - 30\eta^2 + 5\eta^3) - 0.000347341(128 - 640\eta + 720\eta^2 - 280\eta^3 + 35\eta^4) + 0.000133051(-256 + 1920\eta - 3360\eta^2 + 2240\eta^3 - 630\eta^4 + 63\eta^5) \quad (3.6)$$

$$\bar{\phi}(\eta) = 0.110959 - 0.120559(-2+\eta) + 0.0267492(8 - 12\eta + 3\eta^2) - 0.00769854(-16 + 48\eta - 30\eta^2 + 5\eta^3) + 0.000428626(128 - 640\eta + 720\eta^2 - 280\eta^3 + 35\eta^4) - 0.0000606382(-256 + 1920\eta - 3360\eta^2 + 2240\eta^3 - 630\eta^4 + 63\eta^5) \quad (3.7)$$

Unless otherwise stated, the values of thermo-physical parameters for which the procedures are iterated are, $\lambda = Q = A = \beta = Gm = R = 0.2$, $M = 1$, $Kp = 0.5$, $Ec = 0.3$, $Pr = 3$, $\delta = 0.5$, $F_w = 0.1$, $\alpha = \pi/6$, $Gr = 0.5$, $Kn = 2$, $Le = 1$, $e_1 = 0.3$, $e_2 = 0.1$ .The thermo-physical parameter values were chosen based on standard literature references and to realistically simulate engineering scenarios involving non-Newtonian fluids and porous media.

Table 1 validates the accuracy of Legendre collocation method (LCM) compared to the existing findings.

**Table 1: Comparing the values of $-\theta'(0)$ with previous results when $\lambda = R = Ec = M = Kp = \alpha = F_w = A = Q = \delta = 0$**

| Pr | Wang [32] | Gorla and Sidawi [33] | Khan and Pop [34] | Anagandula and Reddy [8] | LCM |
|---|---|---|---|---|---|
| 0.7 | 0.4539 | 0.4539 | 0.4539 | 0.4539 | 0.4544 |
| 2 | 0.9114 | 0.9114 | 0.9113 | 0.9113 | 0.9114 |
| 7 | 1.8954 | 1.8954 | 1.8954 | 1.8954 | 1.8954 |

**Table 2: Comparing Outputs of Skin Friction $-(1 + \frac{\lambda}{2} f''(0))f''(0)$ with varying $Gr$, $Gm$, $M$, and $A$; using Shooting Runge-Kutta Method (SRK) and Legendre Collocation Method (LCM)**

| $Gr$ | $Gm$ | $M$ | $A$ | SRK | LCM |
|---|---|---|---|---|---|
| 0.5 | 0.2 | 2.0 | 0.3 | 0.705607 | 0.707189 |
| 0.7 | 0.2 | 2.0 | 0.3 | 0.638047 | 0.639629 |
| 0.9 | 0.2 | 2.0 | 0.3 | 0.569906 | 0.571488 |
| 0.5 | 0.4 | 2.0 | 0.3 | 0.675857 | 0.677439 |
| 0.5 | 0.6 | 2.0 | 0.3 | 0.646147 | 0.647729 |
| 0.5 | 0.2 | 3.0 | 0.3 | 0.728026 | 0.729608 |
| 0.5 | 0.2 | 4.0 | 0.3 | 0.749376 | 0.750958 |
| 0.5 | 0.2 | 2.0 | 0.4 | 0.630785 | 0.632367 |
| 0.5 | 0.2 | 2.0 | 0.5 | 0.571173 | 0.572755 |

**Table 3: Comparing Outputs of Nusselt Number $-(1 + R)\theta'(0)$ varying $e_1$, $e_2$, $Kp$, and $We$; other values remain the same.**

| $e_1$ | $e_2$ | $Kp$ | $We$ | SRK | LCM |
|---|---|---|---|---|---|
| 0.1 | 0.1 | 0.5 | 3 | 0.436309 | 0.437891 |
| 0.2 | 0.1 | 0.5 | 3 | 0.364149 | 0.365731 |
| 0.3 | 0.1 | 0.5 | 3 | 0.291043 | 0.292625 |
| 0.1 | 0.3 | 0.5 | 3 | 0.256604 | 0.258186 |
| 0.1 | 0.5 | 0.5 | 3 | 0.011936 | 0.011582 |
| 0.1 | 0.1 | 0.7 | 3 | 0.416316 | 0.417898 |
| 0.1 | 0.1 | 0.9 | 3 | 0.397176 | 0.398758 |
| 0.1 | 0.1 | 0.5 | 2 | 0.309088 | 0.310670 |
| 0.1 | 0.1 | 0.5 | 4 | 0.573132 | 0.574704 |

IJMSO
International Journal of Mathematical Sciences and Optimization: Theory and Applications
11(4), 2025, Pages 123 - 137
https://doi.org/10.5281/zenodo.19005495

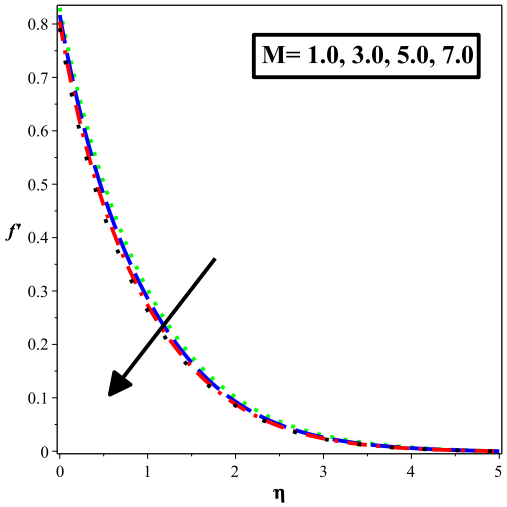


Fig. 2: Effect of $M$ on Velocity profile

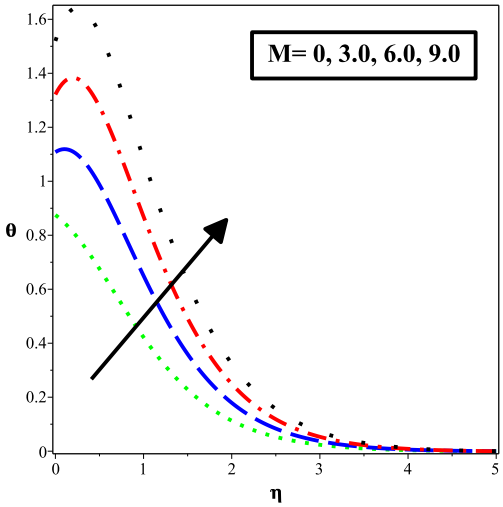


Fig. 3: Effect of $M$ on Thermal profile

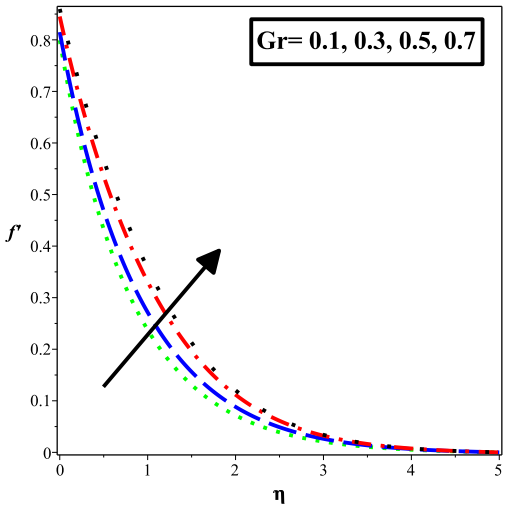


Fig. 4: Effect of $Gr$ on Velocity profile

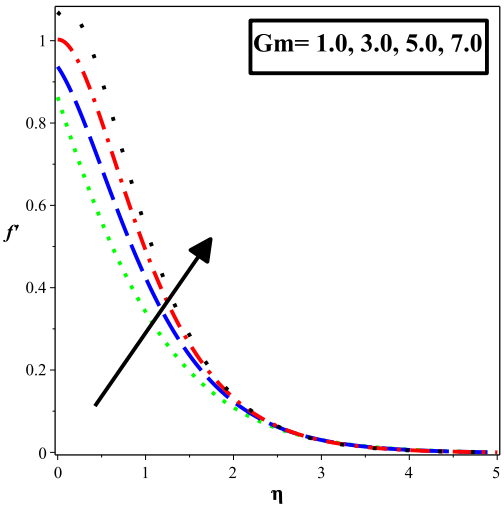


Fig. 5: Effect of $Gm$ on Velocity profile

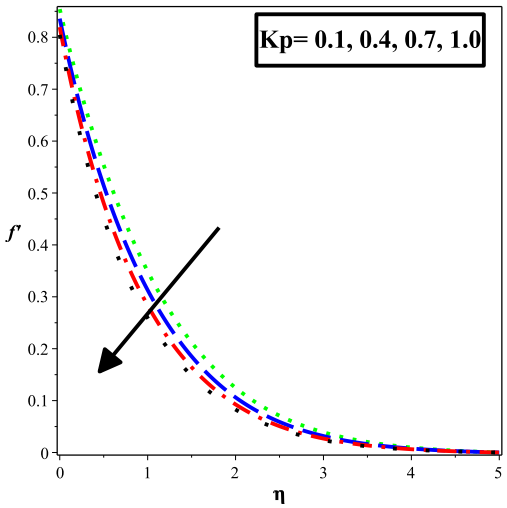


Fig. 6: Impact of $Kp$ on Velocity profile

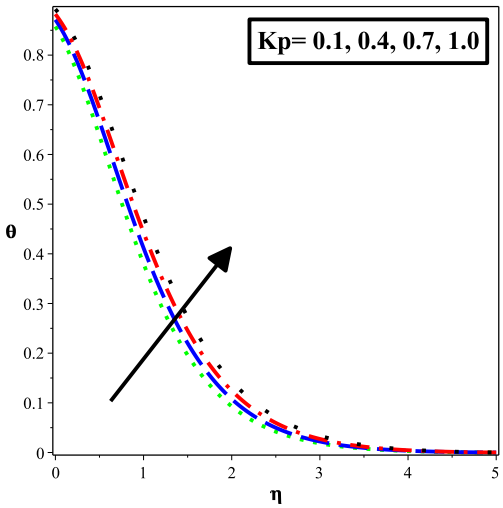


Fig. 7: Impact of $Kp$ on Thermal profile

IJMSO
International Journal of Mathematical Sciences and Optimization: Theory and Applications
11(4), 2025, Pages 123 - 137
https://doi.org/10.5281/zenodo.19005495

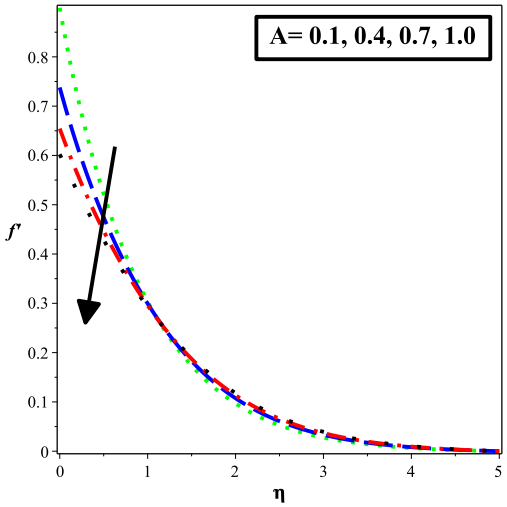


Fig. 8: Effect of $A$ on Velocity profile

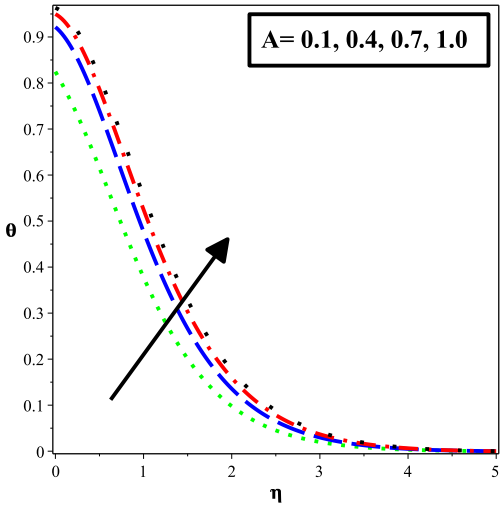


Fig. 9: Effect of $A$ on Thermal profile

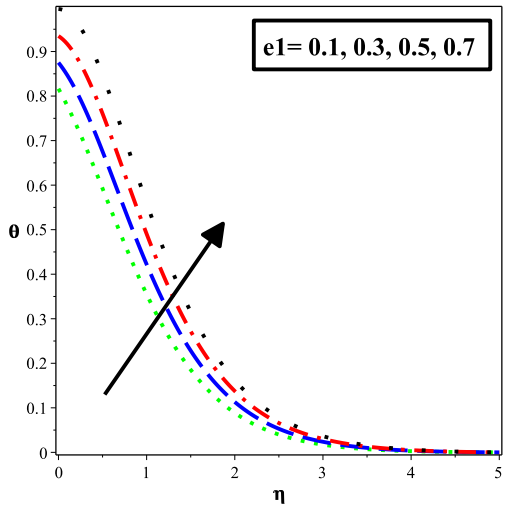


Fig. 10: Impact of $e_1$ on Thermal profile

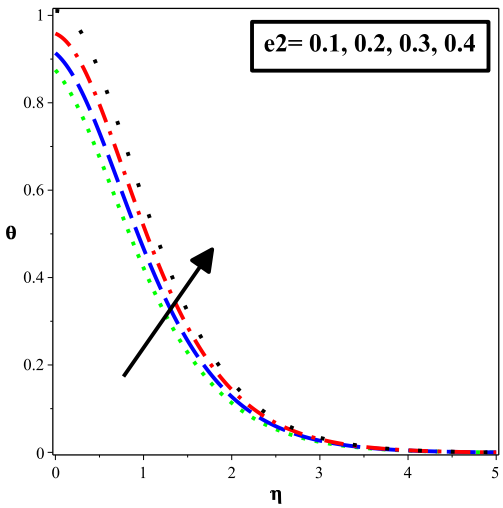


Fig. 11: Impact of $e_2$ on Thermal profile

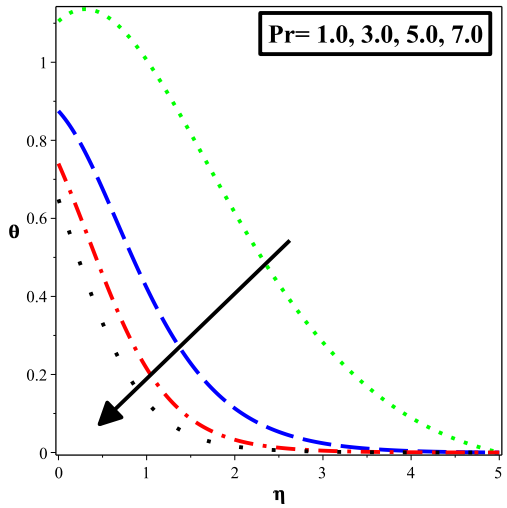


Fig. 12: Influence of $Pr$ on Thermal profile

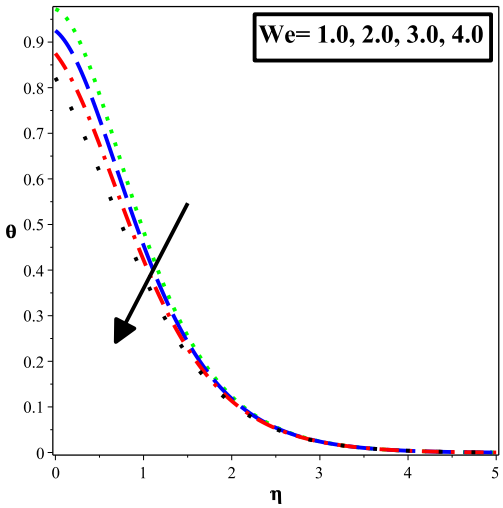


Fig. 13: Influence of $We$ on Thermal profile

IJMSO
International Journal of Mathematical Sciences and Optimization: Theory and Applications
11(4), 2025, Pages 123 - 137
https://doi.org/10.5281/zenodo.19005495

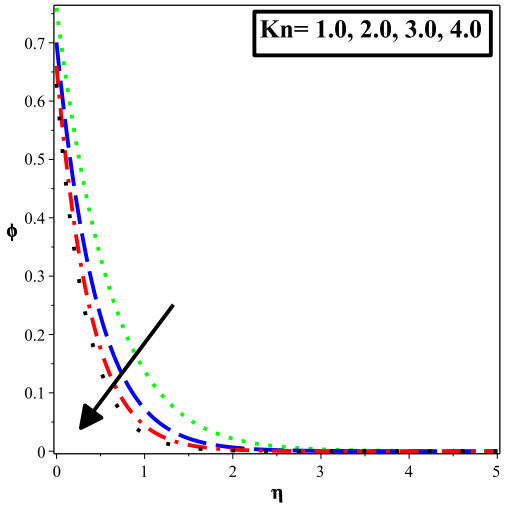


Fig. 14: Effect of $Kn$ on Concentration profile

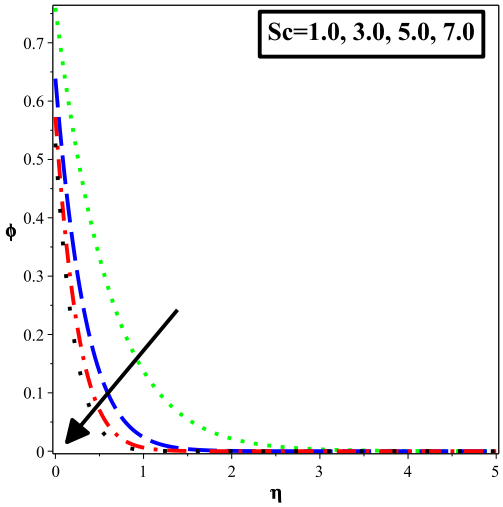


Fig. 15: Effect of $Sc$ on Concentration profile

# 4 Discussion of Results

The effects of various physical parameters on velocity, temperature/thermal, and concentration distributions are showcased through results presented in Tables 2 and 3, as well as Figures 2-15.

Figures 2 and 3 reveal the influence of the magnetic parameter $M$ on the fluid's velocity and temperature profiles respectively. As $M$ increases, the temperature profile rises, which can be attributed to magnetic heating effects within the fluid. In contrast, the velocity profile decreases with a higher magnetic parameter. This occurs due to the Lorentz force, a drag-like resistance that the magnetic field imposes on moving fluid particles, thereby slowing down the flow.

Figure 4 demonstrates the impact of the Grashof number $Gr$ on velocity. An increase in Gr represents stronger buoyancy forces relative to viscous forces, promoting fluid movement. This buoyancy-driven effect enhances circulation and raises the velocity, suggesting that higher Gr leads to more vigorous convection and faster fluid flow.

In Figure 5, the modified Grashof number $Gm$ is shown to similarly affect the velocity profile. As Gm increases, buoyancy further overcomes viscous resistance, resulting in an even greater velocity increase. This trend underscores the role of buoyancy in augmenting flow dynamics within the fluid.

Figures 6 and 7 depict the effects of the porosity parameter $K_p$ on both velocity and temperature. With an increase in $K_p$, the temperature profile rises, indicating enhanced heat retention within the porous medium. However, the velocity profile decreases as $K_p$ increases, highlighting the increased resistance due to the porous structure, which hinders fluid movement.

Figures 8 and 9 examine the effects of the velocity slip parameter $A$ on velocity and thermal profiles. As $A$ rises, temperature shows a noticeable increase. This suggests that a higher velocity slip parameter allows for more efficient energy transfer, thereby elevating the thermal profile.

Figures 10 and 11 illustrate the role of non-uniform heat generation parameters $e_1$ and $e_2$ on the temperature profile. Increases in $e_1$ and $e_2$ intensify the thermal profile, reflecting elevated localized heat within the fluid. This increase results in steeper thermal gradients and temperature peaks, emphasizing the importance of these parameters in controlling thermal stress and ensuring stable heat distribution.

Figure 12 investigates the impact of the Prandtl number $Pr$ on the temperature profile. Higher $Pr$ values reduce the fluid's thermal diffusivity, meaning heat spreads more slowly through the fluid. This results in sharper temperature gradients near the heated surface, indicating that fluids with a higher $Pr$ exhibit more localized heating.

Figure 13 shows the effect of the Weissenberg parameter on the temperature profile. As $We$ increases, the temperature profile decreases. This reduction implies that under greater shear stress,

IJMSO
International Journal of Mathematical Sciences and Optimization: Theory and Applications
11(4), 2025, Pages 123 - 137
https://doi.org/10.5281/zenodo.19005495

the fluid's viscosity drops, which reduces its capacity to retain heat, thereby lowering the temperature distribution.

Figure 14 illustrates the influence of the chemical reaction parameter (Kn) on the concentration profile. With higher values of $Kn$, concentration decreases due to the thinning of the concentration boundary layer. This reduction implies that stronger chemical reactions limit the accumulation of mass within the fluid.

Finally, Figure 15 displays the effect of the Schmidt number $Sc$ on the concentration profile. An increase in $Sc$ reduces the fluid's mass diffusivity, resulting in a lower concentration distribution. This behavior indicates that higher Schmidt numbers limit mass transfer, which lowers concentration within the fluid.

# 5 Conclusion

Although much research exists on Williamson fluid flow, gaps remain in addressing mixed convection, non-uniform internal heat generation, and porous medium effects under an inclined magnetic field. Past studies often assumed uniform heat sources and ignored concentration-driven buoyancy. This study develops a comprehensive model incorporating these factors to better reflect real-world engineering system. By employing a computational approach using Legendre polynomials as basis functions in conjunction with Gauss-Lobatto points, a solution to the nonlinear Williamson fluid model was developed. The findings of this research provide valuable insights into the impact of various parameters on fluid flow. Key outcomes of the study include the following:

- Increase in non-uniform heat generation parameters $e_1$ and $e_2$ raise the thermal profile steeply, intensifying localized heat and steepening thermal gradients. This suggests that regions with higher values of $e_1$ and $e_2$ may experience localized heating, which could influence material stability.
- An increase in the Grashof number enhances the velocity profile, indicating that buoyancy forces contribute significantly to fluid motion as thermal gradients increase.
- Higher porosity leads to a rise in temperature, while the velocity decreases. This indicates that increased porosity improves heat retention in the medium but reduces fluid flow due to greater resistance within the porous structure.
- The Weissenberg parameter, associated with the non-Newtonian properties of Williamson fluid, shows that with an increase in its value, the temperature profile tends to decrease. This reflects the fluid's lower viscosity under shear stress, which reduces thermal retention.

This study, however, has certain limitations. The analysis assumes a steady-state, two-dimensional flow regime, neglects the effects of induced magnetic fields, and models the porous medium as homogeneous and isotropic. The Rosseland approximation was used for radiative heat transfer, simplifying radiative interactions. Future studies could extend the present work by considering unsteady or three-dimensional flows, variable magnetic fields, heterogeneous porous structures, and more complex boundary conditions, such as time-dependent stretching surfaces or non-uniform suction/injection. Furthermore, experimental or numerical validations are recommended to substantiate the theoretical findings presented herein.

IJMSO

International Journal of Mathematical Sciences and Optimization: Theory and Applications
11(4), 2025, Pages 123 - 137
https://doi.org/10.5281/zenodo.19005495

# Nomenclature

| | |
|---|---|
| $U$, $V$ | Velocity components in the $x$ and $y$ directions (m/s) |
| $T$ | Temperature of the fluid (K) |
| $T_w$, $T_\infty$ | Wall and ambient temperatures (K) |
| $C$ | Concentration of the species |
| $C_w$, $C_\infty$ | Wall and ambient concentration |
| $\nu$ | Kinematic viscosity ($m^2/s$) |
| $\rho_f$ | Density of fluid ($kg/m^3$) |
| $\sigma$ | Electrical conductivity (S/m) |
| $\beta_0$ | Magnetic field strength (T) |
| $k$ | Thermal conductivity (W/mK) |
| $C_p$ | Specific heat capacity at constant pressure (J/kgK) |
| $q'''$ | Volumetric rate of heat generation/absorption ($W/m^3$) |
| $g$ | Gravitational acceleration ($m/s^2$) |
| $K^*$ | Permeability of porous medium ($m^2$) |
| $D$ | Mass diffusivity ($m^2/s$) |
| $U_w(x)$ | Stretching velocity, $Uw(x) = bx$ (m/s) |
| $b$ | Stretching rate constant (1/s) |
| $\Gamma$ | Time constant in Williamson model (s) |
| $\alpha$ | Inclination angle of magnetic field |
| $\sigma^*$ | Stefan-Boltzmann constant ($W/m^2K^4$) |
| $k^*$ | Mean absorption coefficient |
| $e_1$, $e_2$ | Space and temperature-dependent heat generation parameters |
| **Dimensionless Parameters** | |
| $M$ | Magnetic parameter |
| $\lambda$ | Williamson parameter |
| $K_p$ | Permeability parameter |
| $We$ | Weissenberg number |
| $Pr$ | Prandtl number |
| $Ec$ | Eckert number |
| $R$ | Radiation parameter |
| $Sc$ | Schmidt number, |
| $Gr$ | Thermal Grashof number |
| $Gm$ | Solutal Grashof number |
| $Kn$ | Chemical reaction parameter |
| $Q$ | Heat source/sink parameter |
| $F_w$ | Suction/injection parameter |
| $A$, $\delta$, $\beta$ | Velocity, thermal, and concentration slip parameters |
| **Similarity Variables** | |
| $\eta$ | Similarity variable |
| $F(\eta)$ | Dimensionless stream function |
| $\theta(\eta)$ | Dimensionless temperature |
| $\phi(\eta)$ | Dimensionless concentration |
| **Engineering Quantities** | |
| $C_f$ | Skin friction coefficient |
| $Nu_x$ | Local Nusselt number (heat transfer rate) |

# References

[1] Mansoor M., Kamran M., Ahmad B., & Ul-Hassan Q. (2022). Non-similar modelling of Williamson fluid over a non-linear stretching sheet with temperature dependent thermal conductivity and chemical reactions. *Zamm - Journal of Applied Mathe-*

*matics and Mechanics / Zeitschrift Für Angewandte Mathematik Und Mechanik, 102*(11). https://doi.org/10.1002/zamm.202200118

[2] Ali A., Ahammad N., Eldin S., Gamaoun F., Daradkeh Y., & Yassen M. (2022). MHD Williamson nanofluid flow in the rheology of thermal radiation, joule heating, and chemical reaction using the Levenberg–Marquardt neural network algorithm. *Frontiers in Energy Research, 10*. https://doi.org/10.3389/fenrg.2022.965603

[3] Alzu'bi O., Alwawi F., Swalmeh M., Sulaiman I., Hamarsheh A., & Ibrahim M. (2022). Energy transfer through a magnetized Williamson hybrid nanofluid flowing around a spherical surface: numerical simulation. *Mathematics, 10*(20), 3823. https://doi.org/10.3390/math10203823

[4] Alwawi F., Faqih F., Swalmeh M., & Ibrahim M. (2022). Combined convective energy transmission performance of Williamson hybrid nanofluid over a cylindrical shape with magnetic and radiation impressions. *Mathematics, 10*(17), 3191. https://doi.org/10.3390/math10173191

[5] Gireesha B. ,Sindhu S.,Sowmya G., & Felicita A. (2020). Magnetohydrodynamic flow of Williamson fluid in a microchannel for both horizontal and inclined loci with wall shear properties. *Heat Transfer, 50*(2), 1428-1442. https://doi.org/10.1002/htj.21937

[6] Rosli W.,Mohamed M.,Sarif N.,Mohammad N., & SoidS. (2022). Blood conveying ferroparticle flow on a stagnation point over a stretching sheet: non-Newtonian Williamson hybrid ferrofluid. *Journal of Advanced Research in Fluid Mechanics and Thermal Sciences, 97*(2), 175-185. https://doi.org/10.37934/arfmts.97.2.175185

[7] Ahmed, K., Akbar, T., & Muhammad, T. (2021). Physical aspects of homogeneous–heterogeneous reactions on MHD Williamson fluid flow across a nonlinear stretching curved surface together with convective boundary conditions. *Mathematical Problems in Engineering, 2021*, 1–13. https://doi.org/10.1155/2021/7016961

[8] Anagandula, S., & Reddy, K. S. (2024). Velocity and thermal slips impact on the Williamson fluid flow above a stretching sheet in the existence of radiation and inclined magnetic field. *CFD Letters, 16*(7), 118–135. https://doi.org/10.37934/cfdl.16.7.118135

[9] Alizadeh, R., Karimi, N., Arjmandzadeh, R., & Mehdizadeh, A. (2018). Mixed convection and thermodynamic irreversibilities in MHD nanofluid stagnation-point flows over a cylinder embedded in porous media. *Journal of Thermal Analysis and Calorimetry, 135*(1), 489–506. https://doi.org/10.1007/s10973-018-7071-8

[10] Ibrahim, W., & Gamachu, D. (2019). Finite element method solution of mixed convection flow of Williamson nanofluid past a radially stretching sheet. *Heat Transfer, 49*(2), 800–822. https://doi.org/10.1002/htj.21639

[11] Maleque, K. (2020). Similarity requirements for mixed convective boundary layer flow over vertical curvilinear porous surfaces with heat generation or absorption. *International Journal of Aerospace Engineering, 2020*, 1–9. https://doi.org/10.1155/2020/7486971

[12] Oderinu, R. A., Ayanbukola, F. J., Alao, S., Sanusi, B. A., & Oyeyinka, T. A. (2025). Mixed convective and nonuniform internal heat generation effect on hydromagnetic micropolar fluid flowing across a permeable stretchy wall: A numerical investigation. *Heat Transfer, 2025*(1). https://doi.org/10.1002/htj.23271

[13] Panezai, A., Rehman, A., Sheikh, N., Iqbal, S., Ahmed, I., Iqbal, M., & Zulfiqar, M. (2019). Mixed convective magnetohydrodynamic heat transfer flow of Williamson fluid over a porous wedge. *American Journal of Mathematical and Computer Modelling, 4*(3), 66. https://doi.org/10.11648/j.ajmcm.20190403.13

[14] Raji, N., Shahabudin, N., Awang, N., Ilias, M., & Ishak, S. (2023). Aligned magnetohydrodynamics mixed convection on various base fluids with carbon nanotubes over an inclined plate. *CFD Letters, 15*(6), 12–25. https://doi.org/10.37934/cfdl.15.6.1225

[15] Akter, R. (2023). Unsteady Williamson fluid flow over exponentially stretching sheet in the presence of non-uniform heat generation or absorption and inclined magnetic field. *Journal of Scientific Research, 15*(3), 621–636. https://doi.org/10.3329/jsr.v15i3.63523

[16] Jyotshna, M., and Dhanalaxmi, V. (2022). Impact of activation energy and heat source or sink on 3D flow of Williamson nanofluid with GaN nanoparticles over a stretching sheet. *European Journal of Mathematics and Statistics, 3*(5), 16–29. https://doi.org/10.24018/ejmath.2022.3.5.133

[17] Alao, S., Oderinu, R. A., Sanusi, B. A., Oyeyinka, T. A., & Ayanbukola, F. J. (2025). Computational investigation of magnetohydrodynamics Casson micropolar fluid flowing past a permeable linearly stretchy wall with heat source. *Journal of the Nigerian Society of Physical Sciences, 7*(3), 2577. https://doi.org/10.46481/jnsps.2025.2577

[18] Kumar, G., Reddy, K., Konijeti, R., & Reddy, M. (2018). Non-uniform heat source or sink and Joule heating effects on chemically radiative MHD mixed convective flow of micropolar fluid over a stretching sheet in porous medium. *Defect and Diffusion Forum, 388*, 281–302. https://doi.org/10.4028/www.scientific.net/DDF.388.281

[19] Raju, C., Sandeep, N., Ali, M., & Nuhait, A. (2019). Heat and mass transfer in three-dimensional MHD Williamson–Casson fluid flow over a stretching surface with non-uniform heat source or sink. *Thermal Science, 23*(1), 281–293. https://doi.org/10.2298/TSCI160426107R

[20] Swain, K., Parida, S., & Dash, G. (2018). Effects of non-uniform heat source or sink and viscous dissipation on MHD boundary layer flow of Williamson nanofluid through a porous medium. *Defect and Diffusion Forum, 389*, 110–127. https://doi.org/10.4028/www.scientific.net/DDF.389.110

[21] Alao, S., Salawu, S. O., Oderinu, R., Oyewumi, A., & Akinola, E. (2024). Viscous heating and thermal gyration of magneto-micropolar fluid particles through an isothermal porous fixed channel with internal non-uniform heat generation: An analytical investigation. *Results in Engineering, 23*, 102474. https://doi.org/10.1016/j.rineng.2024.102474

[22] Jebreen, H. (2023). Solving fractional gas dynamics equation using Müntz–Legendre polynomials. *Symmetry, 15*(11), 2076. https://doi.org/10.3390/sym15112076

[23] Sanusi, B. A., Oderinu, R. A., Alao, S., Ayanbukola, F. J., & Oyeyinka, T. A. (2024). Computational investigation of mixed convective flow of micropolar Casson fluid flowing through a stretchy porous channel with heat source. *Adeleke University Journal of Science, 3*(1). https://aujs.adelekeuniversity.edu.ng

[24] Yousefi, A., Javadi, S., & Babolian, E. (2019). A computational approach for solving fractional integral equations based on Legendre collocation method. *Mathematical Sciences, 13*(3), 231–240. https://doi.org/10.1007/s40096-019-0292-6

[25] Molla, H., & Saha, G. (2019). Numerical approximation of Fredholm integral equation of the second kind using Galerkin and collocation methods. *Ganit: Journal of Bangladesh Mathematical Society, 38*, 11–25. https://doi.org/10.3329/ganit.v38i0.39782

[26] Olabode, B. T., Kayode, S. J., Odeniyan-Fakudade, F. H., & Momoh, A. L. (2024). Numerical solution to singular boundary value problems (SBVPs) using modified linear multistep formulas (LMF). *International Journal of Mathematical Sciences and Optimization: Theory and Applications, 10*(1), 34–52. https://doi.org/10.5281/zenodo.10580147

[27] Binta, B. A., Odekule, M. R., Umar, D., & Waniyos, H. U. (2023). Numerical solution of systems of integro differential equations using polynomial collocation method. *International Journal of Mathematical Sciences and Optimization: Theory and Applications, 9*(2), 44–52. https://doi.org/10.5281/zenodo.10035489

[28] Demir, D., Çınardalı, T., Kürkçü, Ö., & Sezer, M. (2019). The Legendre matrix collocation approach for some nonlinear differential equations arising in physics and mechanics. *European Journal of Science and Technology*, 289–296. https://doi.org/10.31590/ejosat.507708

[29] Alao, S., Salawu, S., Oderinu, R., Oyewumi, A., & Akinola, E. (2024). Investigation of thermal radiation and viscous heating effects on the hydromagnetic reacting micropolar fluid species flowing past a stretchy plate in permeable media. *International Journal of Thermofluids, 22*, 100600. https://doi.org/10.1016/j.ijft.2024.100600

[30] Ayanbukola, F. J., Oderinu, R. A., Alao, S., Oyeyinka, T. A., & Sanusi, B. A. (2024). Theoretical and numerical investigation of thermal radiation in an MHD micropolar fluid flow within a porous channel. *Adeleke University Journal of Science, 3*(1). https://aujs.adelekeuniversity.edu.ng

[31] Akolade, M. T., Adeosun, A. T., & Olabode, J. O. (2021). Influence of thermophysical features on MHD squeezed flow of dissipative Casson fluid with chemical and radiative effects. *Journal of Applied and Computational Mechanics, 7*(4), 1999–2009. https://doi.org/10.22055/JACM.2020.34909.2508

[32] Wang, C. Y. (1989). Free convection on a vertical stretching surface. *ZAMM: Journal of Applied Mathematics and Mechanics / Zeitschrift für Angewandte Mathematik und Mechanik, 69*(11), 418–420. https://doi.org/10.1002/zamm.19890691115

[33] Gorla, R. S., & Sidawi, I. (1994). Free convection on a vertical stretching surface with suction and blowing. *Applied Scientific Research, 52*, 247–257. https://doi.org/10.1007/BF00853952

[34] Khan W. A. & Pop I. (2010). Boundary-layer flow of a nanofluid past a stretching sheet. *International Journal of Heat and Mass Transfer*, 53(11-12), 2477-2483. https://doi.org/10.1016/j.ijheatmasstransfer.2010.01.032